Environment-Assisted Generation of Non-Gaussian Wave-Packet Quantum States

Citation for the original published paper (version of record):
Khanahmadi, M., Mølmer, K. (2026). Environment-Assisted Generation of Non-Gaussian Wave-Packet Quantum States. Physical Review Letters, 137(2). http://dx.doi.org/10.1103/dtd2-4vpn

Environment-Assisted Generation of Non-Gaussian Wave-Packet Quantum States

Maryam Khanahmadi[1,*] and Klaus Mølmer[2]

[1]*Department of Microtechnology and Nanoscience, Chalmers University of Technology, 412 96 Gothenburg, Sweden*

[2]*Niels Bohr Institute, University of Copenhagen, Jagtvej 155A, DK-2200 Copenhagen, Denmark*

(Received 23 April 2025; accepted 4 June 2026; published 7 July 2026)

Generating non-Gaussian states and converting them into traveling wave packets is crucial yet challenging for scalable, fault-tolerant quantum computing. We present a hardware-efficient approach that simultaneously achieves both tasks by combining an engineered nonlinear dissipation with a linear transmission loss from a superconducting circuit to a waveguide. This combination of dissipative channels leverages low-order interactions to induce a high-order nonlinearity, enabling deterministic emission of a wide range of non-Gaussian, error-correctable states, such as Schrödinger cat states, Gottesman-Kitaev-Preskill states, and pair-cat states. We identify experimental superconducting-circuit platforms and realistic parameter regimes for our proposal.

DOI: 10.1103/dtd2-4vpn

Introduction—Encoding quantum information in states that populate propagating wave packets is essential for communication in a quantum internet [1] and for coupling of remote quantum processors in scalable architectures for quantum computing [2]. Using photons or phonons as carriers, the losses in transmission lines, along with decoherence and dephasing errors in the emitters and receivers, limit the fidelity of the desired remote quantum operations. One possibility to overcome these effects is to encode the quantum information in the logical basis of error-correctable quantum states, permitting recovery of the information despite the possible errors [3–5]. Different non-Gaussian bosonic states, such as Schrödinger cat states, binomial states, and Gottesman-Kitaev-Preskill grid states, have been proposed to realize quantum communication and fault-tolerant computing [6–11]. Preparation of quantum information into the logical basis of the Schrödinger cat states has been extensively explored in the optical regimes, either by photon subtraction from squeezed states [12–14] or by utilizing the interaction with single atoms [15,16]. In the microwave regime, the Kerr nonlinearity in Josephson junctions has been used for deterministic generation of cat states in quantum resonator eigenmodes [17–20].

Previous works have explored architectures that include a tunable coupler to transfer the prepared stationary state to a waveguide [2,3,21,22]. Such couplers may introduce unwanted nonlinear interactions, and the longer duration of the separate preparation and release processes reduces the output quantum-state fidelity due to dissipation. In this Letter, we directly generate traveling non-Gaussian states by parametric driving of a nonlinear resonator undergoing constant linear loss to a transmission waveguide. In this approach, the release is faster, and the profile of the parametric drive determines the shape of the propagating wave packet and eliminates the need for tunable couplers.

Unitary preparation of an n-legged cat state requires a nonlinear interaction proportional to $\hat{a}^{\dagger n}\hat{a}^n$ [$(2n)$th order of nonlinearity in field amplitude operators]. A procedure based on such interactions has been analyzed in the Kerr-parametric oscillator [23]. As an alternative approach, one may obtain nonlinear effects from an engineered dissipative coupling, n-photon decay to the environment [24–26]. The use of dissipation to generate nonclassical states and achieve steady-state entanglement in stationary modes has been proposed and demonstrated in various quantum systems [27,28], and preparation of stationary bosonic states has been extensively studied both theoretically [29–33] and experimentally [34–36]. In this Letter, we demonstrate that an engineered nonlinear dissipation channel can affect a quantum bosonic system such that its linear emission into a waveguide forms high-fidelity propagating quantum states in single wave-packet modes. Our theory thus marks a significant step toward the development of hardware-efficient quantum processors for long-distance communication.

Cat state in a resonator mode—Following [18,19,37], we consider a single oscillator mode, described by the Lindblad master equation $\dot{\hat{\varrho}} = -i[\hat{H}, \hat{\varrho}] + \kappa\mathcal{D}(\hat{L})\hat{\varrho}$ where $\mathcal{D}(\hat{L})\hat{\varrho} = \hat{L}\,\hat{\varrho}\,\hat{L}^\dagger - \frac{1}{2}\{\hat{L}^\dagger\hat{L}, \hat{\varrho}\}$, κ is a dissipation rate, and the Hamiltonian $\hat{H}$ and Lindblad operator L are expressed in terms of the ladder operators $(\hat{a}, \hat{a}^\dagger)$. Considering the Hamiltonian $\hat{H} = \Omega_d(\hat{L} + \hat{L}^\dagger)$, the master equation can be

*Contact author: m.khanahmadi@chalmers.se

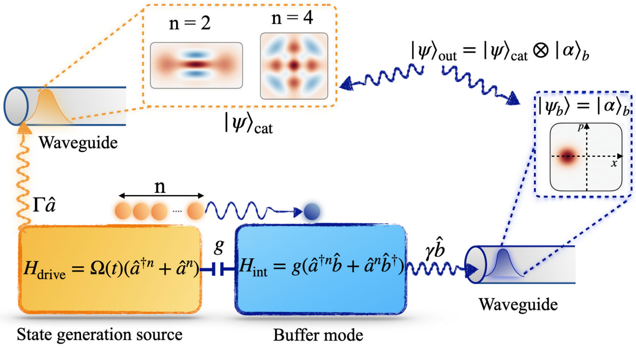

FIG. 1. Combination of engineered nonlinear dissipation and linear dissipation for the preparation of traveling cat-state wave packets. The cat state is generated in the output field of the a mode, SGS (orange box). The buffer b mode (blue box) is coupled to the SGS through the "n-to-1-photon" interaction H_{int}. Both modes undergo strong linear transmission, Γ and γ, into two separate waveguides. The total output field consists of a cat state $|\psi\rangle_{\text{cat}}$ in the left waveguide and a coherent state $|\alpha\rangle_b$ in the right waveguide. The entire system is initialized in the vacuum state, and the time-dependent drive $\Omega(t)$ shapes the output wave-packet mode.

written in the compact form $\dot{\varrho} = \kappa\mathcal{D}(\hat{L} - \lambda)\hat{\varrho}$ which has the stable steady state satisfying $\hat{L}\varrho_{\text{steady}} = \lambda\varrho_{\text{steady}}$, where $\lambda = e^{(i3\pi/2)}(2\Omega_d/\kappa)$ is the eigenvalue corresponding to the eigenstate of $\hat{L}$. A linearly driven and damped oscillator ($\hat{L} = \hat{a}$) has a coherent steady state, while assuming $\hat{L} = \hat{a}^2$ or $\hat{L} = \hat{a}^4$ leads to the steady-state generation of two or four different coherent states (the solutions to $\alpha^n = \lambda$) and their Schrödinger cat superposition states [18,19,37].

The n-photon loss $\hat{L} \propto \hat{a}^n$ can be accomplished by engineering the interaction with a second, so-called "buffer mode" through the interaction Hamiltonian $\hat{H}_{\text{int}} = g_{ab}(\hat{a}^n\hat{b}^\dagger + \hat{a}^{\dagger n}\hat{b})$; cf. the schematics shown in Fig. 1. The buffer mode with field operators $\{\hat{b}, \hat{b}^\dagger\}$ is strongly coupled with rate γ to a waveguide through a linear loss Lindblad operator $\hat{L}_b = \sqrt{\gamma}\hat{b}$, and when $\gamma \gg g_{ab}$, the buffer mode can be adiabatically eliminated: $\dot{b} = -ig_{ab}a^n - (\gamma/2)b \approx 0 \Rightarrow b = (-i2g_{ab}a^n/\gamma)$. This results in the effective Lindblad master equation on the desired form, $\dot{\varrho} = (4g_{ab}^2/\gamma)\mathcal{D}(\hat{a}^n - \alpha^n)\hat{\varrho}$, where $\lambda = \alpha^n = e^{(i3\pi/2)}(\Omega_d\gamma/2g_{ab}^2)$. The engineered anticommutator loss term in the master equation corresponds to the evolution by a non-Hermitian Hamiltonian $\hat{H} \propto i\hat{L}^\dagger\hat{L} \approx i\hat{a}^{\dagger n}\hat{a}^n$ and thus a $(2n)$th-order nonlinearity in field amplitude operators, resulting from an only $(n+1)$st-order interaction with the buffer mode.

Cat state in a wave-packet mode—Introducing a constant linear loss with rate Γ into a waveguide turns the oscillator into a state generating source (SGS), releasing the oscillator field to a traveling wave-packet mode whose shape is controlled by the time-dependent drive $\Omega_d(t)$. Assuming that the coupling to the waveguide is weak, and that $\Omega_d(t)$ varies slowly, the intracavity field will adiabatically follow the steady-state solution of $(4g_{ab}^2/\gamma)\mathcal{D}[\hat{a}^n - \alpha(t)^n]\hat{\varrho} = 0$ with $\alpha(t)^n = e^{(i3\pi/2)}[\Omega_d(t)\gamma/2g_{ab}^2]$. Because of the linear loss, the time-dependent amplitude of the emitted field follows the intracavity amplitude, and emission into a specifically desired mode function $\propto \alpha(t)$ is enabled by applying the corresponding time-dependent drive strength, $\Omega_d(t) = e^{(-i3\pi/2)}(2g_{ab}^2/\gamma)\alpha(t)^n$. For drive pulses of finite duration, nonadiabatic corrections will cause the emitted mode to differ from the desired shape $\alpha(t)$ and the quantum state to differ from the desired cat quantum state. We compensate these effects in parts by a counterdiabatic correction [38] to the drive amplitude; see Supplemental Material for more details [39].

We examine the dynamics obtained, without adiabatic elimination of the buffer mode, by solving the master equation of the combined system, shown in Fig. 1,

$$\dot{\varrho} = -i\left[\Omega_d(t)(\hat{a}^n + \hat{a}^{\dagger n}) + g_{ab}(\hat{a}^n\hat{b}^\dagger + \hat{a}^{\dagger n}\hat{b}), \hat{\varrho}\right] + \gamma\mathcal{D}(\hat{b})\hat{\varrho} + \Gamma\mathcal{D}(\hat{a})\hat{\varrho}. \tag{1}$$

With realistic parameters for superconducting-circuit platforms and with the driving field $\Omega_d(t)$ appropriately adjusted by the counterdiabatic correction, we verify that the emitted microwave field with a very high fidelity populates the single wave-packet mode cat state specified by our simple analysis.

In the full system, the SGS and the buffer-mode field become entangled by their high-order interaction, and the field lost through the buffer mode could cause decoherence of the wave-packet quantum state. However, our simulation shows that the buffer-mode output separates from the SGS output, and, moreover, that it occupies a single-mode coherent state with high fidelity, so that quantum jumps associated with the detection of photons from the buffer mode have no effect on the state of the system.

Multimode analysis of the output field—To investigate the SGS output field character, we utilize the master equation (1) and the quantum regression theorem to evaluate the autocorrelation function and the mode decomposition of the emitted field, see End Matter. This analysis serves to validate that the output field almost exclusively populates a single time-dependent mode function. We find, indeed, that only small deviations are visible between the precise shape of the most occupied mode $v_1(t)$ and the temporal shape $\alpha(t)$, and that the cat-state fidelity of the mode directly controlled by the drive $\Omega_d(t)$ is high in all our calculations for the two-legged cat-state protocol. For the four-legged cat-state protocol, the cat-state fidelity is high in the most occupied mode $v_1(t)$; however, to have the least deviation as a two-legged cat state, a correction of the drive amplitude must be applied to control the wave-packet shape.

Experimental proposal—In this section, we present a superconducting-circuit implementation of Eq. (1); see Ref. [39] for details. In this platform, controlling the interaction between microwave photons relies on Josephson junction (JJ) elements to implement nonlinear dynamics through the potential $U(\hat{\varphi}) \propto E_J[1 - \cos(\hat{\varphi})]$, where $\hat{\varphi}$ is the phase across the junction with the junction energy E_J [43]. The JJ acts as a nonlinear inductance, and its response can be tuned *in situ* by applying a phase bias, which is achieved by threading a magnetic flux Φ through a superconducting loop including the JJs. The flux drive can be tuned to implement particular interactions and avoid escape to unconfined states. In our proposal, we utilize an asymmetrically threaded superconducting quantum interference device (SQUID) (ATS) [34] that consists of a SQUID, including two JJs with junction energies E_1, E_2 in parallel, shunted in the center by a large inductance L_J. This device comprises two loops with the corresponding flux drives φ_1, φ_2, respectively; see Sec. A in [39].

We consider a symmetric SQUID, i.e., $E_1 = E_2 = E_J$, with the nonlinear potential of the ATS obtained as $\hat{U}(\hat{\varphi}) \propto 2E_J \cos(\varphi_\Sigma)\cos(\hat{\varphi} + \varphi_\Delta)$, where $2\varphi_\Sigma = \varphi_1 + \varphi_2$ and $2\varphi_\Delta = \varphi_1 - \varphi_2$. To suppress the dominant self-Kerr and cross-Kerr resonant interactions, we assume the difference between the two dc bias drives is $\varphi_\Delta = \pi/2$. Then, the Hamiltonian of the ATS depends only on the nonlinear odd terms of the flux operator $\hat{H} \propto \sin(\hat{\varphi}) \propto \sum_k \hat{\varphi}^{2k+1}$. Finally, the flux drive $\varphi_\sum$ is adjusted to implement the interaction needed [44,45].

The full circuit follows the ATS design for both SGS and buffer modes, which are capacitively coupled. By adjusting a flux drive on the buffer-mode ATS with the frequency $\propto n\boldsymbol{\omega}_a - \boldsymbol{\omega}_b$ and introducing an n-photon drive on the SGS-ATS through the charge line $\propto [\hat{\boldsymbol{a}}^\dagger e^{in\omega_a t} + \text{H.c.}]$, the effective Hamiltonian of the circuits is evaluated as $\hat{H}_{\text{eff}} = \Omega_n(t)(\hat{\boldsymbol{a}}^n + \hat{\boldsymbol{a}}^{\dagger n}) + g_n(\hat{\boldsymbol{a}}^n\hat{\boldsymbol{b}}^\dagger + \hat{\boldsymbol{a}}^{\dagger n}\hat{\boldsymbol{b}})$, where the coefficients $\Omega_n(t), g_n$ depend on the circuit parameters; see Ref. [39]. By coupling the SGS and buffer mode to the waveguides, the dynamics of the quantum circuit can be described by the evolution in Eq. (1). It is worth noting that, compared to recent papers on stabilizing the two-legged cat state [19,30,34,35], they consider a linear resonator as a storage cavity and apply both drives on the buffer mode. However, in our proposal, we use a separate ATS for the SGS and apply only the n-photon decay to the buffer mode for two important reasons. First, this prevents the transition of photons from the b mode to the SGS and then into the waveguide, ensuring that the output field only populates a single-mode wave packet. Second, since we generate and release the state in the same process, we do not rely on long storage and coherence times of the resonator.

Simulation results—As discussed, the SGS is subject to a linear and an effective nonlinear dissipation channel with rates Γ and $\kappa_n = 4g_{ab}^2/\gamma$, which must be properly balanced to produce the high-fidelity cat states. In Fig. 2, we show the fidelity and size of cat states obtained for various combinations of decay rates and coupling strengths. In both panels, the color represents the ratio κ_n/Γ, cf. the right color bar, and the numbers indicated above the filled circles inside each panel box correspond to g_{ab}/γ. For each set of parameters, we identify the value of $\alpha = \alpha_{\text{out}}$ maximizing the state fidelity $F = \langle\psi|\hat{\varrho}_{\text{out}}|\psi\rangle$ of the two- and four-legged cat state. In the resulting (α_{out}, F) plot, we see that the fidelity is in the range of 95% or more for cat state sizes relevant for quantum communication and computing. The insets in the figure show the Wigner functions of the smallest and largest cat states generated.

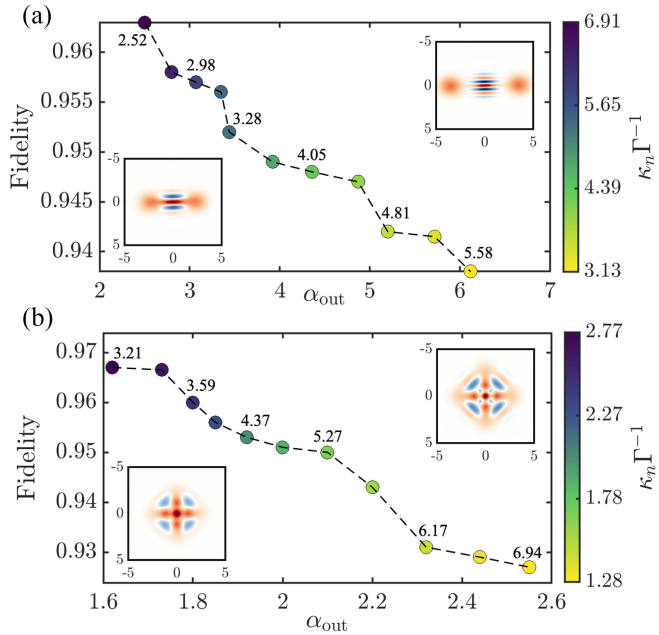

FIG. 2. The fidelity of the output field two- and four-legged cat states is shown in panel (a) and (b), respectively, with the corresponding achievable amplitude parameters α_{out} together with the corresponding achievable amplitude parameters α_{out}. The relative values of the coupling and dissipation rate γ/g_{ab} are indicated by the number on several filled circles in each panel. The color bar indicates the ratio between linear Γ and nonlinear dissipation κ_n. The left and right insets show the Wigner function of the highest and lowest fidelity two- and four-legged cat states (here, and in all figures, the Wigner functions are rotated to align with the real and imaginary axes).

State transformations in the cat state qubit basis—The Hamiltonian in Eq. (1) and the Lindblad damping operators commute with the parity operator $\hat{P} = (-1)^{\hat{a}^\dagger\hat{a}}$, so that starting from the vacuum state, the dynamics is restricted to the even-parity subspace. Thus, we prepare two- and four-legged even cat states with equal amplitudes on coherent states $|C_\alpha^{+2}\rangle = \mathcal{N}(|\alpha\rangle + |-\alpha\rangle)$ and $|C_\alpha^{+4}\rangle = \mathcal{N}(|\alpha\rangle + |-\alpha\rangle + |i\alpha\rangle + |-i\alpha\rangle)$, respectively. Defining these as logical qubit $|0\rangle$ states, to encode a qubit, we need a protocol to prepare also the respective logical qubit $|1\rangle$

states (odd cat-state basis), $|C_\alpha^{-2}\rangle = \mathcal{N}(|\alpha\rangle - |-\alpha\rangle)$ and $|C_\alpha^{-4}\rangle = \mathcal{N}[|\alpha\rangle + |-\alpha\rangle - (|i\alpha\rangle + |-i\alpha\rangle)]$ and qubit superposition states. To this end, we note that a linear or parametric drive, $\hat{V} = \epsilon p(t)(\hat{a}^{(n/2)} + \hat{a}^{\dagger(n/2)}), n = 2(4)$, executes a rotation in the two- (four-) legged cat-state qubit space because of the dissipative suppression of state components outside this space. Considering the projection operators in the basis of the cat state qubit $\hat{\Pi}^{\pm n} = |C^{\pm n}\rangle\langle C^{\pm n}|, n = 2,\ 4$, the interaction can be written $\epsilon p(t)(\hat{\Pi}^{+n} + \hat{\Pi}^{-n})(\hat{a}^{(n/2)} + \hat{a}^{\dagger(n/2)})(\hat{\Pi}^{+n} + \hat{\Pi}^{-n}) = \Omega_x(|C^{+n}\rangle\langle C^{-n}| + |C^{-n}\rangle\langle C^{+n}|)$, where $\Omega_x = 2\epsilon p(t)|\alpha|^{(n/2)}$ denotes the coherent coupling between the logical cat state qubits. The dissipative suppression of transitions out of the qubit space requires $|\epsilon p(t)| \ll |\alpha|^2\kappa_n$; see Refs. [18,37] for more details. In our numerical analysis, we assume the same drive profile as in Eq. (1), with the additional requirement $\epsilon \ll \Omega$, and we find that the added drive does not alter the buffer-mode output state, and we can therefore apply the qubit rotation and produce high-fidelity cat state qubit superposition states in outgoing single-mode wave packets.

Figures 3(a) and 3(b) show the Wigner functions of the most populated mode, revealing the expected two- and four-legged cat state qubit superposition states, respectively. The states are ideally of the form $\sqrt{p_+}|C_\alpha^{+n}\rangle + e^{i\phi}\sqrt{p_-}|C_\alpha^{-n}\rangle$. The state shown in Fig. 3(a) has a fidelity of 95.3% with the cat-state qubit superposition state with parameters $p_+ = 0.75$, $p_- = 0.25$, $\phi = 0.52\pi$, and $|\alpha|^2 = 2.52$, with a Wigner function shown in Fig. 3(c). The state shown in Fig. 3(b) has a 94.5% fidelity with the four-legged cat superposition with parameters $p_+ = 0.9$, $p_- = 0.1$, $\phi = 1.5\pi$, and $|\alpha|^2 = 1.85$, with the Wigner function shown in Fig. 3(d). It is important to note that the two-legged cat state can be generated faster than the four-legged cat state, as it only requires a third-order nonlinearity. Hence, we obtain higher fidelity, in general, for the two-legged cat state than the four-legged cat state. For the details of the parameters of the circuits, we refer the reader to Appendix B in [39]. Considering values of $\Gamma^{-1} = 0.22$ and 1.32 μs, the total generation times obtained from Fig. 3 are approximately $T \approx 2$ and 9.3 μs for the two and four cat states, respectively; see Supplemental Material [39] for more details.

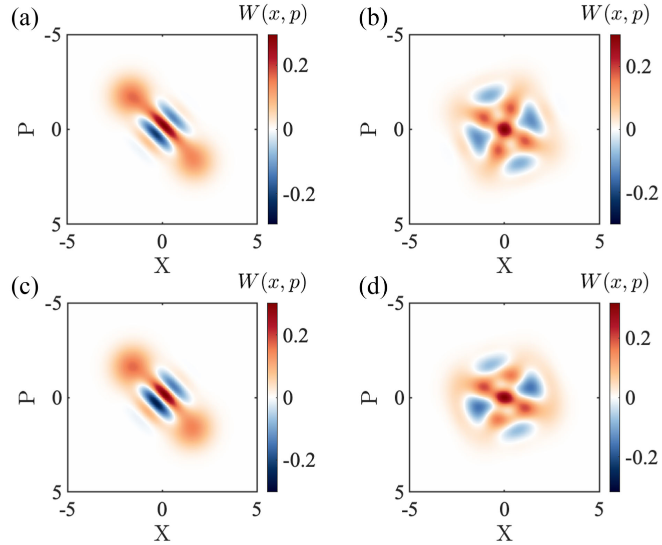

FIG. 3. A two- (four-) legged cat-state qubit superposition state generated with the simulation parameters $\kappa_n/\Gamma = 6.9(2.0)$ and rotating drive strength $\epsilon/\Omega = 5\%(8\%)$ is displayed in (a),(b). The corresponding ideal cat-state qubit superposition state is displayed in (c),(d). The cat state amplitudes and state fidelities are presented in the text.

Summary—We have demonstrated a deterministic and hardware-efficient method for generating propagating Schrödinger cat states using superconducting circuits. By engineering two- and four-photon loss, we have shown that it is possible to produce high-fidelity two- and four-component cat states in single traveling wave-packet modes, controlled by the shape of a classical driving pulse. Our calculations show that the emission into the buffer-mode reservoir is well approximated by a single wave-packet mode coherent state. This implies that the system is always in an eigenstate of the buffer-mode jump operator $\sqrt{\gamma}\hat{b}$, and hence the state evolution is governed exclusively by the no-jump $(2n)$th order non-Hermitian term $\propto i\hat{a}^{\dagger n}\hat{a}^n$, arising from the interaction with the buffer mode. We have also shown that, by applying a simultaneous linear or quadratic drive, we can rotate the cat state qubit superposition states, which is essential for applications in quantum communication and computing.

As an important application of our proposal, we have also studied the generation of propagating grid states from propagating four cat states, marking a significant step toward large-scale fault-tolerant quantum communication and computing. As detailed in Supplemental Material [39], our theory also extends to the generation of entangled propagating states, such as pair-cat states. We further note that propagating non-Gaussian quantum states may also serve as sensitive probes for metrological purposes [46–49].

The state generation source and the buffer mode may both be subjected to additional noises, e.g., dephasing and other dissipation channels. Because of the simultaneous generation and release of the quantum states, our approach will, however, be less sensitive to such effects than preparation methods that rely on storage and subsequent release of the quantum state. Looking ahead, controlling higher-order terms in the expansion of the Josephson nonlinearities and utilizing optimal control may enable even faster preparation and higher-fidelity cat state qubit states than the approach presented here and relying on approximations and low-order interactions [50].

Acknowledgments—M. K. acknowledges fruitful discussions with G. Johansson and useful comments from S. Girvin and T. Hillmann. This work was supported by the

Knut and Alice Wallenberg Foundation through the Wallenberg Center for Quantum Technology (WACQT) and the Danish National Research Foundation Center for Quantum Hybrid Networks (No. DNRF 139). The numerical simulations were performed using resources provided by the Chalmers Center for Computational Science and Engineering (C3SE) under project 2025/1 − 6.

Data availability—The data that support the findings of this article are not publicly available. The data are available from the authors upon reasonable request.

[1] H. J. Kimble, Nature (London) **453**, 1023 (2008).

[2] P. Campagne-Ibarcq, E. Zalys-Geller, A. Narla, S. Shankar, P. Reinhold, L. Burkhart, C. Axline, W. Pfaff, L. Frunzio, R. J. Schoelkopf, and M. H. Devoret, Phys. Rev. Lett. **120**, 200501 (2018).

[3] C. J. Axline, L. D. Burkhart, W. Pfaff, M. Zhang, K. Chou, P. Campagne-Ibarcq, P. Reinhold, L. Frunzio, S. Girvin, L. Jiang *et al.*, Nat. Phys. **14**, 705 (2018).

[4] P. Kurpiers, M. Pechal, B. Royer, P. Magnard, T. Walter, J. Heinsoo, Y. Salathé, A. Akin, S. Storz, J.-C. Besse, S. Gasparinetti, A. Blais, and A. Wallraff, Phys. Rev. Appl. **12**, 044067 (2019).

[5] J. Yang, M. Khanahmadi, I. Strandberg, A. Gaikwad, C. Castillo-Moreno, A. F. Kockum, M. A. Ullah, G. Johansson, A. M. Eriksson, and S. Gasparinetti, Phys. Rev. Lett. **134**, 240803 (2025).

[6] Z. Leghtas, G. Kirchmair, B. Vlastakis, R. J. Schoelkopf, M. H. Devoret, and M. Mirrahimi, Phys. Rev. Lett. **111**, 120501 (2013).

[7] L. Li, C.-L. Zou, V. V. Albert, S. Muralidharan, S. M. Girvin, and L. Jiang, Phys. Rev. Lett. **119**, 030502 (2017).

[8] B. M. Terhal, J. Conrad, and C. Vuillot, Quantum Sci. Technol. **5**, 043001 (2020).

[9] K. Noh and C. Chamberland, Phys. Rev. A **101**, 012316 (2020).

[10] A. Joshi, K. Noh, and Y. Y. Gao, Quantum Sci. Technol. **6**, 033001 (2021).

[11] J. E. Bourassa, R. N. Alexander, M. Vasmer, A. Patil, I. Tzitrin, T. Matsuura, D. Su, B. Q. Baragiola, S. Guha, G. Dauphinais *et al.*, Quantum **5**, 392 (2021).

[12] A. Ourjoumtsev, R. Tualle-Brouri, J. Laurat, and P. Grangier, Science **312**, 83 (2006).

[13] K. Wakui, H. Takahashi, A. Furusawa, and M. Sasaki, Opt. Express **15**, 3568 (2007).

[14] T. Serikawa, J. I. Yoshikawa, S. Takeda, H. Yonezawa, T. C. Ralph, E. H. Huntington, and A. Furusawa, Phys. Rev. Lett. **121**, 143602 (2018).

[15] S. Deleglise, I. Dotsenko, C. Sayrin, J. Bernu, M. Brune, J.-M. Raimond, and S. Haroche, Nature (London) **455**, 510 (2008).

[16] B. Hacker, S. Welte, S. Daiss, A. Shaukat, S. Ritter, L. Li, and G. Rempe, Nat. Photonics **13**, 110 (2019).

[17] B. Vlastakis, G. Kirchmair, Z. Leghtas, S. E. Nigg, L. Frunzio, S. M. Girvin, M. Mirrahimi, M. H. Devoret, and R. J. Schoelkopf, Science **342**, 607 (2013).

[18] M. Mirrahimi, Z. Leghtas, V. V. Albert, S. Touzard, R. J. Schoelkopf, L. Jiang, and M. H. Devoret, New J. Phys. **16**, 045014 (2014).

[19] M. Mirrahimi, C.R. Phys. **17**, 778 (2016).

[20] X. He, Y. Lu, D. Bao, H. Xue, W. Jiang, Z. Wang, A. Roudsari, P. Delsing, J. Tsai, and Z. Lin, Nat. Commun. **14**, 6358 (2023).

[21] W. Pfaff, C. J. Axline, L. D. Burkhart, U. Vool, P. Reinhold, L. Frunzio, L. Jiang, M. H. Devoret, and R. J. Schoelkopf, Nat. Phys. **13**, 882 (2017).

[22] M. Khanahmadi, M. M. Lund, K. Mølmer, and G. Johansson, Phys. Rev. Res. **5**, 043071 (2023).

[23] H. Goto, Z. Lin, T. Yamamoto, and Y. Nakamura, Phys. Rev. A **99**, 023838 (2019).

[24] F. Verstraete, M. M. Wolf, and J. Ignacio Cirac, Nat. Phys. **5**, 633 (2009).

[25] Y. Liu, S. Shankar, N. Ofek, M. Hatridge, A. Narla, K. M. Sliwa, L. Frunzio, R. J. Schoelkopf, and M. H. Devoret, Phys. Rev. X **6**, 011022 (2016).

[26] E. Kapit, Quantum Sci. Technol. **2**, 033002 (2017).

[27] F. Reiter, L. Tornberg, G. Johansson, and A. S. Sørensen, Phys. Rev. A **88**, 032317 (2013).

[28] D. D. Bhaktavatsala Rao and K. Mølmer, Phys. Rev. Lett. **111**, 033606 (2013).

[29] M. Wolinsky and H. J. Carmichael, Phys. Rev. Lett. **60**, 1836 (1988).

[30] Z. Leghtas, S. Touzard, I. M. Pop, A. Kou, B. Vlastakis, A. Petrenko, K. M. Sliwa, A. Narla, S. Shankar, M. J. Hatridge *et al.*, Science **347**, 853 (2015).

[31] F. Minganti, N. Bartolo, J. Lolli, W. Casteels, and C. Ciuti, Sci. Rep. **6**, 26987 (2016).

[32] S. Touzard, A. Grimm, Z. Leghtas, S. O. Mundhada, P. Reinhold, C. Axline, M. Reagor, K. Chou, J. Blumoff, K. M. Sliwa, S. Shankar, L. Frunzio, R. J. Schoelkopf, M. Mirrahimi, and M. H. Devoret, Phys. Rev. X **8**, 021005 (2018).

[33] P. M. Harrington, E. J. Mueller, and K. W. Murch, Nat. Rev. Phys. **4**, 660 (2022).

[34] R. Lescanne, M. Villiers, T. Peronnin, A. Sarlette, M. Delbecq, B. Huard, T. Kontos, M. Mirrahimi, and Z. Leghtas, Nat. Phys. **16**, 509 (2020).

[35] U. Réglade, A. Bocquet, R. Gautier, J. Cohen, A. Marquet, E. Albertinale, N. Pankratova, M. Hallén, F. Rautschke, L.-A. Sellem *et al.*, Nature (London) **629**, 778 (2024).

[36] A. Marquet, S. Dupouy, U. Réglade, A. Essig, J. Cohen, E. Albertinale, A. Bienfait, T. Peronnin, S. Jezouin, R. Lescanne, and B. Huard, Phys. Rev. Appl. **22**, 034053 (2024).

[37] R. Gautier, A. Sarlette, and M. Mirrahimi, PRX Quantum **3**, 020339 (2022).

[38] A. del Campo, Phys. Rev. Lett. **111**, 100502 (2013).

[39] See Supplemental Material at http://link.aps.org/supplemental/10.1103/dtd2-4vpn for detailed derivations and additional discussion, which includes Refs. [40–42].

[40] S. E. Nigg, H. Paik, B. Vlastakis, G. Kirchmair, S. Shankar, L. Frunzio, M. H. Devoret, R. J. Schoelkopf, and S. M. Girvin, Phys. Rev. Lett. **108**, 240502 (2012).

[41] A. Vanselow, B. Beauseigneur, L. Lattier, M. Villiers, A. Denis, P. Morfin, Z. Leghtas, and P. Campagne-Ibarcq, Phys. Rev. X **16**, 011032 (2026).

[42] K. Takase, F. Hanamura, H. Nagayoshi, J. E. Bourassa, R. N. Alexander, A. Kawasaki, W. Asavanant, M. Endo, and A. Furusawa, Phys. Rev. A **110**, 012436 (2024).

[43] M. H. Devoret and J. M. Martinis, *Experimental Aspects of Quantum Computing* (Springer, New York, 2005), p. 163.

[44] A. Miano, G. Liu, V. Sivak, N. Frattini, V. Joshi, W. Dai, L. Frunzio, and M. Devoret, Appl. Phys. Lett. **120**, 184002 (2022).

[45] R. Lescanne, L. Verney, Q. Ficheux, M. H. Devoret, B. Huard, M. Mirrahimi, and Z. Leghtas, Phys. Rev. Appl. **11**, 014030 (2019).

[46] K. Duivenvoorden, B. M. Terhal, and D. Weigand, Phys. Rev. A **95**, 012305 (2017).

[47] M. Khanahmadi and K. Mølmer, Phys. Rev. A **107**, 013705 (2023).

[48] L. Gravina, F. Minganti, and V. Savona, PRX Quantum **4**, 020337 (2023).

[49] D. Gottesman, A. Kitaev, and J. Preskill, Phys. Rev. A **64**, 012310 (2001).

[50] I. Rojkov, M. Simoni, E. Zapusek, F. Reiter, and J. Home, Phys. Rev. X **16**, 011056 (2026).

[51] H.-P. Breuer and F. Petruccione, *The Theory of Open Quantum Systems* (Oxford University Press, Oxford, 2002).

[52] C. Gardiner and P. Zoller, *Quantum Noise: A Handbook of Markovian and Non-Markovian Quantum Stochastic Methods with Applications to Quantum Optics* (Springer, New York, 2004).

[53] A. H. Kiilerich and K. Mølmer, Phys. Rev. Lett. **123**, 123604 (2019).

[54] J. Combes, J. Kerckhoff, and M. Sarovar, Adv. Phys. X **2**, 784 (2017).

[55] D. J. Weigand and B. M. Terhal, Phys. Rev. A **97**, 022341 (2018).

[56] B. Q. Baragiola, G. Pantaleoni, R. N. Alexander, A. Karanjai, and N. C. Menicucci, Phys. Rev. Lett. **123**, 200502 (2019).

[57] C. Vuillot, H. Asasi, Y. Wang, L. P. Pryadko, and B. M. Terhal, Phys. Rev. A **99**, 032344 (2019).

[58] P. Campagne-Ibarcq, A. Eickbusch, S. Touzard, E. Zalys-Geller, N. E. Frattini, V. V. Sivak, P. Reinhold, S. Puri, S. Shankar, R. J. Schoelkopf *et al.*, Nature (London) **584**, 368 (2020).

[59] M. V. Larsen, C. Chamberland, K. Noh, J. S. Neergaard-Nielsen, and U. L. Andersen, PRX Quantum **2**, 030325 (2021).

[60] A. L. Grimsmo and S. Puri, PRX Quantum **2**, 020101 (2021).

[61] K. Noh, C. Chamberland, and F. G. S. L. Brandão, PRX Quantum **3**, 010315 (2022).

[62] V. V. Albert, K. Noh, K. Duivenvoorden, D. J. Young, R. T. Brierley, P. Reinhold, C. Vuillot, L. Li, C. Shen, S. M. Girvin, B. M. Terhal, and L. Jiang, Phys. Rev. A **97**, 032346 (2018).

[63] Y. Zheng, A. Ferraro, A. F. Kockum, and G. Ferrini, Phys. Rev. A **108**, 012603 (2023).

[64] G. S. Agarwal, J. Opt. Soc. Am. B **5**, 1940 (1988).

[65] S.-C. Gou, J. Steinbach, and P. L. Knight, Phys. Rev. A **54**, 4315 (1996).

[66] V. V. Albert, S. O. Mundhada, A. Grimm, S. Touzard, M. H. Devoret, and L. Jiang, Quantum Sci. Technol. **4**, 035007 (2019).

[67] M. Yuan, Q. Xu, and L. Jiang, Phys. Rev. A **106**, 062422 (2022).

[68] J. M. Gertler, S. van Geldern, S. Shirol, L. Jiang, and C. Wang, PRX Quantum **4**, 020319 (2023).

End Matter

Appendix A: Analysis of the SGS output field—To investigate the output field from the SGS, we simulate Eq. (1) and use the quantum regression theorem [51,52] to evaluate the autocorrelation function $\mathcal{G}^{(1)}(t_1, t_2) = \kappa\langle\hat{a}^\dagger(t_1)\hat{a}(t_2)\rangle = \kappa\mathrm{Tr}(\hat{a}^\dagger\mathcal{L}(t_2, t_1)(\hat{a}\mathcal{L}(t_1, 0)\hat{\varrho}(0)))$, where $\mathcal{L}(t', t)$ denotes the linear time evolution map of the master equation (1) from time t to t' and $\hat{\varrho}(0)$ denotes the initial vacuum state of the system and buffer modes.

When evaluated on a temporal grid, $\mathcal{G}^{(1)}(t_1, t_2)$ constitutes a matrix that we diagonalize to identify the mode decomposition $\mathcal{G}^{(1)}(t_1, t_2) = \sum_i n_i v_i^*(t_1) v_i(t_2)$, where $\{v_i(t)\}$ are orthonormal temporal modes of the output field with corresponding mean photon number n_i. The aim of our protocol is that the output field of the SGS populates only one mode $v(t)$ that is determined by the classical drive amplitude, $v(t) \simeq \alpha(t) \propto \Omega_d(t)^{1/n}$. Our numerical analysis confirms that the overlap $|\int\tilde{\alpha}(t)^* v_1(t) dt|$ between the normalized desired mode $\tilde{\alpha}(t) = \sqrt{\mathcal{N}}\alpha(t)$ and the most populated mode $v_1(t)$ typically exceeds 0.99 for the two-legged cat states. The similar values are typically 0.96 or above for the four-legged cat states.

The state fidelities and the Wigner functions provided in the figures in the main text of the Letter refer to the quantum states populating the most occupied single-mode component of the output field $[v(t) = v_1(t)]$, which is, for the two-legged cat states, practically indistinguishable from the population of the mode $\tilde{\alpha}(t)$, while a correction of the drive amplitude $\Omega_d(t)$ may be needed to prepare a four-legged cat state in an output wave packet of our own choice.

To calculate the quantum state populating an arbitrary wave-packet mode $v(t)$, we follow Ref. [53] and determine the state of the field building up in an artificial downstream cavity with ladder operators $\{\hat{d}, \hat{d}^\dagger\}$. Such a cavity will fully capture the quantum-state contents of the mode $v(t)$, if its coupling to the wave guide is $g_v(t) = -v^*(t)/\sqrt{\int_0^t |v(t)|^2}$, and we recover the quantum state (reduced density matrix) of the wave-packet mode by solving the cascaded systems master equation including $\hat{H}_{da}(t) = i(\sqrt{\Gamma}/2)[g_v^*(t)\hat{a}^\dagger\hat{d} - g_v(t)\hat{d}^\dagger\hat{a}]$ and $\hat{L}_{sv} = \sqrt{\Gamma}\hat{a} + g_v^*(t)\hat{d}$ [53,54].

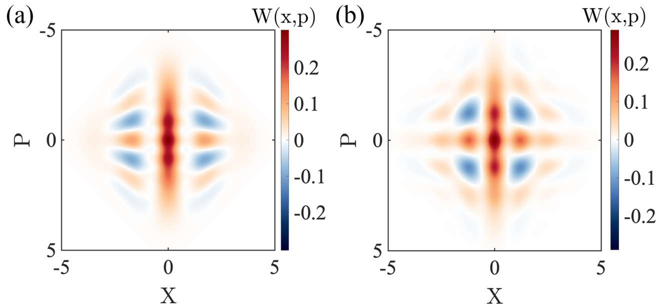

FIG. 4. (a),(b) The Wigner distribution of the propagating grid state obtained by the first and second iteration of the breeding protocol on the generated four cat state with fidelity 95% with $|\alpha|^2 \approx 2.1$, respectively. The effective squeezing parameters $\Delta_x = 3.6$ and $\Delta_p = 1.1$ dB along the x and p axes, respectively, are evaluated for (b).

To determine the characteristics of the signal emitted by the buffer mode, we evaluate the autocorrelation function $\mathcal{G}^{(1)}(t_1, t_2) = \gamma\langle\hat{b}^\dagger(t_1)\hat{b}(t_2)\rangle$. Using the mode decomposition, we find an all-dominant single buffer-mode output field, and with the cascaded-system formalism, we find that the output has a very high overlap of 0.99 (0.985) with a coherent state with amplitude −3.85 (−2.39) in the case of the two- (four-) legged cat state protocols presented in Fig. 3.

Appendix B: Application: Propagating grid states—A significant example of propagating non-Gaussian quantum states is the traveling grid state, which serves as an ideal state for sensing purposes and also as an important resource for obtaining fault-tolerant quantum computing and error correction [8,49,55–61]. Our theory enables the breeding of wave-packet quantum states, which can be combined on beam splitters and subjected to measurements of x or p quadratures that herald the presence of grid states in definite temporal modes in the unmeasured output port. While [62,63] suggest preparing grid states by breeding from binomial states $\propto |0\rangle + |4\rangle$, we breed from four-legged cat state with dominant $|0\rangle$ and $|4\rangle$ components when $|\alpha|^2 \approx 2.1$. The Wigner functions after one and two iterations of the beam splitter and quadrature measurement on one output port are shown in Figs. 4(a) and 4(b); see Ref. [39] for further details.

Appendix C: Extension to entangled-state wave packets: Generation of pair-cat states—Our theoretical approach can be generalized for the preparation of multimode entangled states, particularly pair-cat states [64–68], which occupy wave packets traveling in different waveguides or different frequencies. For this to work, the wave packets are released from two distinct resonator modes with field operators $\{\hat{a}_1, \hat{a}_2\}$ and resonance frequencies $\{\boldsymbol{\omega}_{\boldsymbol{a}_1}, \boldsymbol{\omega}_{\boldsymbol{a}_2}\}$, respectively; see Fig. 3 in Supplemental Material [39]. These modes are both coupled to the SGS and buffer mode of Fig. 1, causing correlated losses described by the master equation $\dot{\varrho} = \kappa\mathcal{D}(\hat{L} - \lambda)\hat{\varrho}$, with $\hat{L} \propto \hat{a}_1^2\hat{a}_2^2$. The steady-state solutions of this equation are the so-called pair-coherent states $|\alpha, \alpha\rangle_{a_1,a_2} \propto \sum_n(\alpha^{2n}/n!)|n, n\rangle$, and superposition states such as the "pair-cat state" with only even numbered Fock state components, $|\text{pair cat}\rangle \propto |\alpha, \alpha\rangle_{a_1,a_2} + |i\alpha, i\alpha\rangle_{a_1,a_2}$ [39]. These states can protect effective two-qubit entanglement and exponentially suppress dephasing errors and arbitrary photon loss in both modes [66].

Implementation of the joint Lindblad operator $\hat{L}_{12} \propto \hat{a}_1^2\hat{a}_2^2$ can be achieved by a flux drive on the buffer mode with a frequency $\omega_d = \boldsymbol{\omega}_{\boldsymbol{b}} - 2(\boldsymbol{\omega}_{\boldsymbol{a}_1} + \boldsymbol{\omega}_{\boldsymbol{a}_2})$ and on the SGS with the frequency $\propto 2(\boldsymbol{\omega}_{\boldsymbol{a}_1} + \boldsymbol{\omega}_{\boldsymbol{a}_2})$, which lead to the effective Hamiltonian $\hat{H}_{\text{eff}}^{\text{pair}} = \Omega_d(t)(\hat{a}_1^2\hat{a}_2^2 + \text{H.c.}) + g(\hat{a}_1^2\hat{a}_2^2 b^\dagger + \text{H.c.})$; see the details in Supplemental Material [39], Sec. D. To simultaneously release the entangled state into wave-packet modes in two wave guides, we consider the same constant decay rate for both modes, $\hat{L}_{a_1} = \sqrt{\Gamma}\hat{a}_1, \hat{L}_{a_2} = \sqrt{\Gamma}\hat{a}_2$, i.e., in Eq. (1) the SGS dissipation changes as $\Gamma\mathcal{D}(\hat{a})\hat{\varrho} \rightarrow \Gamma\mathcal{D}(\hat{a}_2)\hat{\varrho} + \Gamma\mathcal{D}(\hat{a}_1)\hat{\varrho}$. We assume the temporal profile similar to Fig. 3(b) with a rescaled amplitude with maximum $(\text{drive}/\Gamma) = 1.3$ and total pump duration $3.5/\Gamma$. Using the simulation parameter $\gamma/g_{ab} = 7.2, 4g_{ab}^2/\Gamma\gamma = 1.2$, we obtain 96% of the output fields in a single mode, with the fidelity $F = 95\%$ to a pair-cat state with $|\alpha|^2 = 0.94$ during the total evolution time $T = 6/\Gamma$. This high fidelity is promising for the sharing of entanglement and information between distant quantum processors. For the details of the drive shape and the relevant parameters, check Appendixes B and D in [39].